ISSN: 0067-2904

Ecofriendly Synthesis of ZnO Nanoparticles using Zingiber Officinale and Syzygium Aromaticum Extracts for Antibacterial Applications

M. J. Tuama and M.F.A.Alias*
Physics Department, College of Science, University of Baghdad, Jadariya, Baghdad, Iraq

Received: 13/2/2023 Accepted: 23/10/2023 Published: 10/9/2024

Abstract

Zinc oxide nanoparticles (ZnO NPs) were prepared by green method using Zingiber officinale (G-ZnO) and Syzygium aromaticum extract (S-ZnO). X-ray diffraction (XRD) investigations revealed that ZnO NPs have wurtzite hexagonal structures in extracts of Zingiber officinale and Syzygium aromaticum, with average crystal sizes of about 38.49 nm and 27.66 nm, respectively. FTIR was performed to investigate the nature of functional groups in the active compounds responsible for the formation of ZnO NPs. The diffuse reflection spectroscopy (DRS) showed the direct bandgap energy of the as-prepared nanoparticles. The zinc oxide sample composition and purity were confirmed using energy dispersive X-ray spectroscopy (EDX). The morphological properties of ZnO NPs prepared from both plants were investigated using scanning electron microscopy (SEM). G-ZnO and S-ZnO nanoparticles appeared agglomerated of triangular, spherical and various other shapes, respectively. The average size of nanoparticles for G-ZnO and S-ZnO NPs were 26.92 nm and 62.45 nm, respectively. In addition, the as-prepared ZnO NPs showed significant bactericidal effects against gram-positive and gram-negative pathogenic bacteria.

Keywords: Green synthesis, Zinc oxide nanoparticles, Zingiber officinale, Syzygium aromaticum, antibacterial application.

تحضير جسيمات اوكسيد الزنك النانوية الصديقة للبيئة باستخدام مستخلصات الزنجبيل و القرنفل للتطبيقات المضادة للبكتيريا

محمد جمعة طعمة , ميسون فيصل احمد الياس*
قسم الفيزياء ، كلية العلوم ،جامعة بغداد، الجادرية ، بغداد،العراق

الخلاصة

تم تحضير جزيئات أوكسيد الزنك النانوية (ZnO NPs) بالطريقة الخضراء باستخدام مستخلص الزنجبيل والقرنفل . اوضحت فحوصات حيود الاشعة السينية أن جزيئات أوكسيد الزنك النانوية لها هياكل سداسية في المستخلص النباتي للزنجبيل والقرنفل وبمتوسط حجم بلوري 38.49 و27.66 نانومتر على التوالي. تم إجراء مطيافية فوريه لتحويل الأشعة تحت الحمراء للتحقق من طبيعة المجموعات الوظيفية في المركبات النشطة المسؤولة عن تكوين جزيئات أوكسيد الزنك النانوية. أظهر طيف الانعكاس المنتشر أن فجوة الطاقة كانت مباشرة للجسيمات النانوية المحضرة. تم معرفة نقاوة و محتوى أكسيد الزنك لكل عينة باستخدام التحليل

*Email: may20131313@yahoo.com

الطيفي المشتت للطاقة. تم فحص خصائص المورفولوجية لجزيئات أوكسيد الزنك النانوية المحضرة من كلا النباتين باستخدام المجهر الإلكتروني الماسح حيث اظهرت تجمعات مع اشكال مثلثة وكروية لكل من G–ZnO و S–Zn وان معدل الحجم للجسيمات النانوية 26.92 نانومتر و 62.45 نانومتر على التوالي ، أظهرت جزيئات أوكسيد الزنك النانوية المحضرة لها تأثيرا ضد البكتيريا الموجبة والسالبة الجرام.

1. Introduction

Nanotechnology has extended the potential to provide innovative technology for the utilization of new nanomaterials in numerous industrial, biological and medical areas [1-4]. Nano particels (NPs) may be synthesized following physical-chemical methods [5,6] but they are expensive, bad for the environment, and needs a lot of energy. Environmentally friendly processes were used to create different metal oxide nanoparticles [7]. Affordable and ecologically responsible methods for creating nanoparticles than chemical and physical processes have been suggested, known as the green syntheses. Green synthesis strategy combines plants with salts such as nitrates, chlorides, or sulfates in order to produce nanoparticles [8]. Plant extract contains phytochemicals that function as capping agents and reducing agents. Several plant components, including leaves, stems, fruits, seeds, roots, and flower buds, have been employed to producte different nanoparticles [9]. Natural chemicals found in biological systems have a crucial and multifaceted function in creating nanoparticles and serve as capping agents to stabilize them. Using plants has significant benefits over other biological systems. Plants are readily available, safe to handle, and produce more stable nanoparticles than other sources of nanomaterials [10,11].

An area of nanoscience and nanotechnology that is expanding is the green production of metal and metal oxide nanoparticles (NPs) [12,13]. Zinc oxide nanoparticles are among the most important metal oxide nanoparticles because of their distinctive shape (size, shape, and crystalline structure), low toxicity, economic aspect, and biocompatibility [14,15]. Nanoparticles may exhibit antibacterial activity through various mechanisms, including the release of antibacterial metal ions from the surface of the particle and the antimicrobial activity associated with the physical properties of the nanoparticles related to cell wall penetration or membrane damage[16].

This research paper aims to prepare and characterize ZnO nanoparticles using Zingiber officinale and Syzygium aromaticum extracts by the green method and assess their antibacterial activity for human applications.

2. Experimental Part

The ginger plant roots (Zingiber officinale) and Syzygium aromaticum flower buds (clove) were purchased from the local market and washed thoroughly with triple distilled water. Zinc nitrate hexahydrate $Zn(NO_3)_2.6H_2O$ and (NH_4OH) ammonium hydroxide were purchased from the Alpha Chemika India company, and deionized water (DW) was used. With an electric grinder, Zingiber officinale roots and Syzygium aromaticum flower buds were ground, and their powder was stored in plastic containers. A regulated amount of distilled deionized water (1:10) was added to the plant powder, i.e. 10 mL of water per 1 gram of plant, and stirred vigorously for 30 min at 70 °C. Whatman filter No.1 paper was used to filter out the extracts, and the filtrate was then kept in a refrigerator at 4 °C [17]. Each extract was prepared separately, as shown in Figure 1.

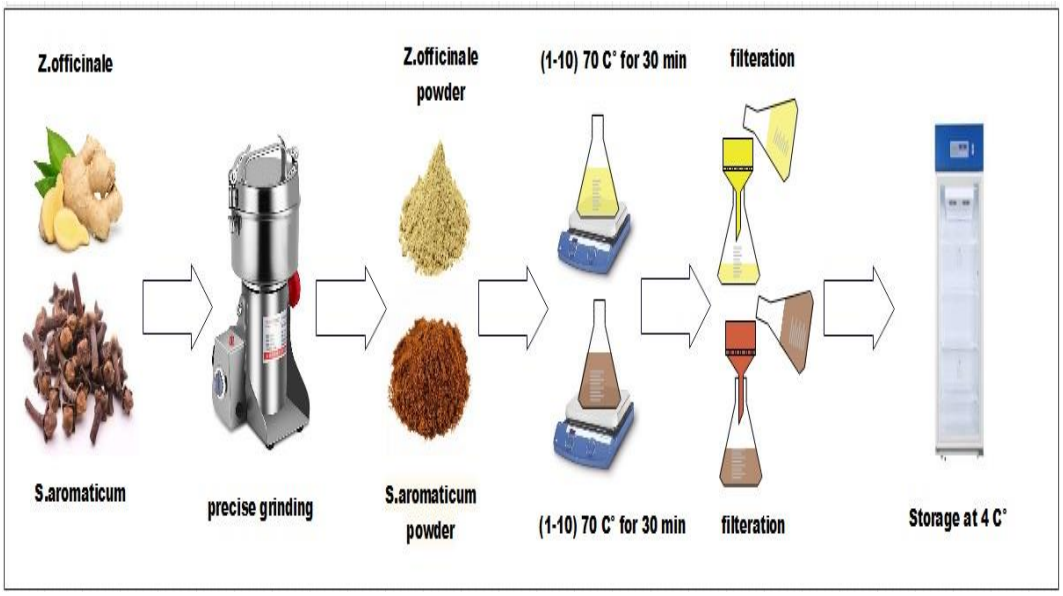

Figure 1: Steps involved in creating aqueous extracts of Z. Officinale ground root and Syzygium aromaticum flower buds.

ZnO NPs were produced utilizing a green method by adding zinc nitrate hexahydrate to 100 ml DW to reach a concentration of (1M), adding 25 ml of plant extract, followed by (NH_4OH) of 98% purity, and agitating the mixture on a magnetic stirrer at 70-80°C for 1h. The sediment was centrifuged for 15 minutes at 4,000 rpm. Several washings were done with DW to achieve a pH of 7 [18]. The resulting mixture was then put into a crucible and heated to 400 °C for two hours (see Figure 2) [1,19]. The green synthesis of ZnO NPs using root Zingiber officinale (G-ZnO) and Syzygium aromaticum (S-ZnO) was according to the following chemical reactions:

$$Zn(NO_3)_2 \cdot 6H_2O + NH_4OH + \text{plant extract} \rightarrow \text{Zn(OH)}_2 \downarrow + NH_4NO_3 + \text{plant extract}$$

$$\text{Plant extract} + \text{Zn(OH)}_2 \xrightarrow{400°C} \text{ZnO NPs (caooed with phyto} - \text{molecules)} + H_2O$$

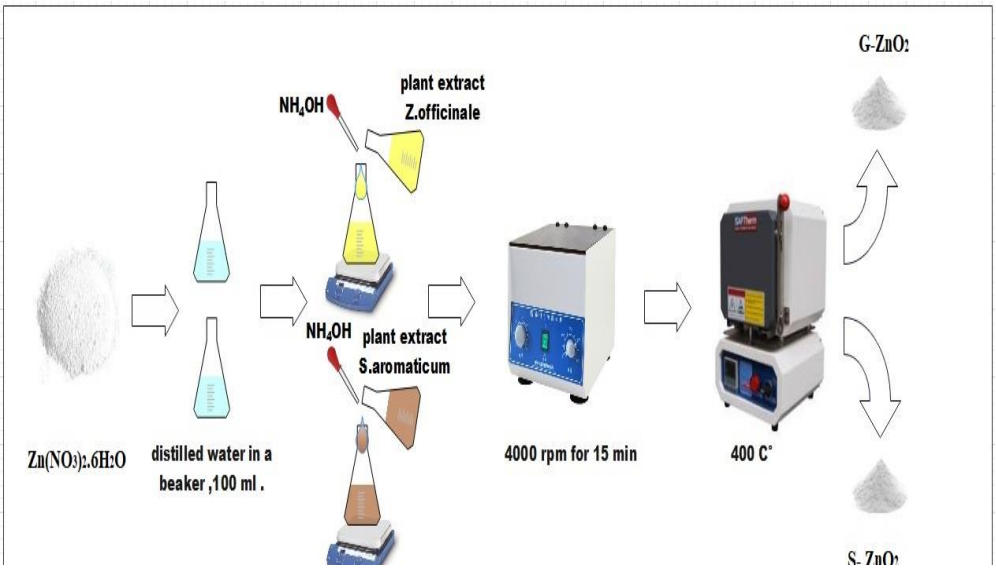

Figure 2 : Production of Zno nanoparticles utilizing the green synthesis method

The as-prepared ZnO nanoparticles were characterized using X-ray diffraction techniques to confirm their presence, structure and crystallite size. Fourier Transform Infrared (FTIR) spectroscopy was used to identify the functional groups in the plant extract involved in the bonding process with ZnO NPs. In addition for the characterization and identification of organic and inorganic substances and biomolecules, the extract has emerged as a reducing agent and capping agent.

Diffuse reflection spectroscopy (DRS) was used to determine the optical properties, energy dispersive X-ray spectroscopy (EDX) was used to find the composition of the prepared samples, and scanning electron microscopy (SEM) was used to identify the morphological properties of the prepared nanoparticles.

Microbial susceptibility to nanoparticles was determined using Mueller-Hinton agar. The antibacterial activity of G-ZnO NPs and S-ZnO NPs against Staphylococcus aureus (S. aureus), Escherichia coli (E. coli) , and Bacillus subtilis (B. subtilis) was tested as well as the agar spread technique. The Mueller-Hinton agar was prepared according to the manufacturer's instructions, sterilized at 121°C for 15 min in petri dishes, and was left to solidify. Using the standard Macckfer land technique, the nocturnal turbidity of S. aureus, E. coli, and B. subtilis growths was approximated to 10^8 CFU/ml. A cotton swab was soaked in each bacterial growth under investigation, wiped on the surface of Müller-Hinton agar, and left for 30 min at 25 °C. 6 mm holes were punched with a needle using a cork borer and filled with 100 µl of (G-ZnO and S-ZnO) NPs at concentrations of 100 µg/mL. All plates were incubated at 37°C for 24-72 hours, and the radius of the inhibition zones in mm was recorded to examine which nanomaterials had better antibacterial efficiency.

3. Results and Discussion

Figure 3 shows the X-ray diffraction (XRD) patterns of G-ZnO and S-ZnO powders. The patterns indicated polycrystalline with hexagonal wurtzite structure for all the prepared samples. Table 1 gives the structural and geometric parameters. The XRD pattern for G-ZnO NPs (Figure 3A) has peaks at 2θ = 31.76°,34.47°, 36.23°, 47.45°, 56.61°, 62.85°, 66.39°, 67.96°, 69.1°, 72.56°, and 77.01°corresponding to (100), (002), (101), (012), (110), (013), (200), (112), (201), (004) and (202) planes, respectively, which matched the data of JCPDS card: (96-901-1663).

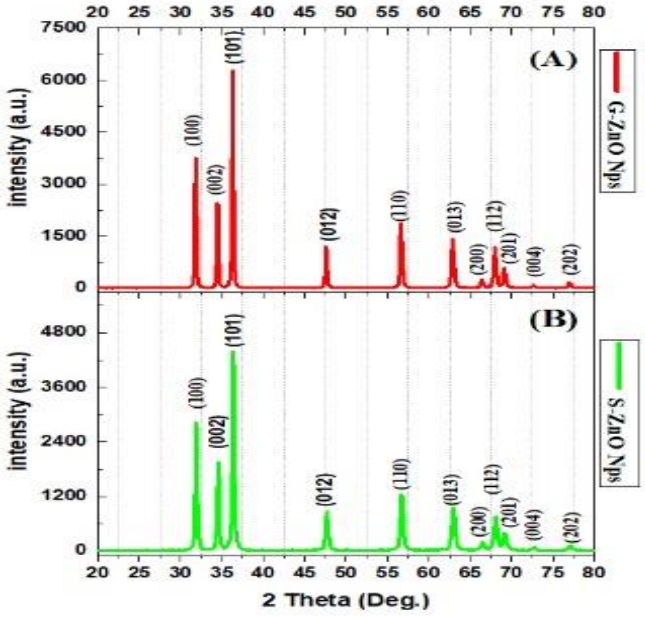

Figure 3: XRD spectra of (A) G-ZnO NPs and (B) S-ZnO NPs

The XRD pattern of S-ZnO NPs, shown in Figure 3B and Table 1, shows that Syzygium aromaticum extract has peaks at 2θ = 31.78°, 34.43°, 36.23°, 47.54°, 56.56°, 62.38°, 66.32°, 67.92°, 69.02°, 72.57°, and 77.94° corresponding to planes (100), (002), (101), (012), (110), (013), (200), (112), (201), (004) and (202), respectively, which matched the data of JCPDS card: (96-900-4182). The crystallite size of each of the G- ZnO NPs and S-ZnO NPs, given in Table 1, was obtained from the XRD study data[20], whereas the average crystallite size for G-ZnO NPs and S- ZnO NPs of 38.49 nm and 27.66 nm, respectively were calculated using the Scherrer formula[20, 21]:

$$D = k\lambda / \beta \cos\theta \qquad 1$$

Where: D is the crystallite size of the crystal, k is Scherrer's constant (0.9), λ is X-ray wavelength (0.15406 nm), ß is the width of the XRD peak at half height, and Θ is the Bragg diffraction angle [21]. The acquired XRD results for G-ZnO and S-ZnO nanoparticles are in good agreement with those that have been published in prior studies [22, 23].

Table : 1 G-ZnO and S-ZnO NPs structure and geometric parameters characteristics.

G-ZnO NPs					
2θ (Deg.)	**FWHM (Deg.)**	**dhkl Exp.(Å)**	**C.S (nm)**	**dhkl Std.(Å)**	**hkl**
31.76	0.2	2.815182269	41.29748594	2.8137	100
34.47	0.15	2.599804223	55.45185093	2.603	002
36.23	0.2	2.477444231	41.79293864	2.4654	101
47.45	0.25	1.914515282	34.7106532	1.9109	012
56.61	0.2	1.624539832	45.11565412	1.6245	110
62.85	0.3	1.477419587	31.03274083	1.4772	013
66.39	0.3	1.406965823	31.64505336	1.4068	200
67.96	0.3	1.378234394	31.9342964	1.3782	112
69.1	0.3	1.358253857	32.15146629	1.3581	201
72.56	0.2	1.301772142	49.27394387	1.3017	004
77.01	0.35	1.23726489	29.00499334	1.2377	202
average crystaline size (nm)			38.491916	JCPDS card.(96-901- 1663)Hexagonal	
S-ZnO NPs					
2θ (Deg.)	**FWHM (Deg.)**	**dhkl Exp.(Å)**	**C.S (nm)**	**dhkl Std.(Å)**	**hkl**
31.78	0.2498	2.813456213	33.06608258	2.8174	100
34.43	0.2498	2.602733018	33.29414544	2.8037	002
36.23	0.2998	2.477444231	27.88054612	2.478	101
47.54	0.3497	1.911100605	24.82316935	1.9122	012
56.56	0.3497	1.625857236	25.79643076	1.6266	110
62.38	0.4496	1.487416782	20.65531091	1.4778	013
66.32	0.4496	1.408280967	21.10703979	1.4087	200
67.92	0.4496	1.378948637	21.30346102	1.3795	112
69.02	0.4496	1.359632709	21.44307786	1.3598	201
72.57	0.1998	1.301617404	49.32642701	1.3018	004
77.94	0.3997	1.224810935	25.56432025	1.239	202
average crystaline size (nm)			27.66000101	JCPDS card.(96-900-4182)Hexagonal	

The solid phase ZnO samples were examined by FTIR within the range of 400-4000 cm^{-1} and using the KBr pellet method to identify organic and inorganic biomolecule residues from the
nanoparticles, which may come along via reducing agents on the surface of ZnO NPs. Furthermore, the plant extract's functional groups involved in the process of binding with ZnO NPs were discovered. Figure 4 and Table 2 compare the FTIR spectra of the Zingiber officinale plant extract with that of the biosynthesized ZnO NPs. Zingiber officinale also contains aldehydes, phenols, and ketone monomers [24] .

The effectiveness of Zingiber officinale extract as a reducing agent and a covering agent was confirmed by FTIR screening of G-ZnO NPs. Broadband coupling at 3439 cm^{-1} means broadband (OH) expansion vibrations. The peaks were observed at 2980, 1579, 1420, 1036, 630, and 465 cm^{-1}, and the wave numbers and their functional groups were assigned as given in Table 2. One can see from Figure 4, the presence of organic compounds, various types of polyphenols, carboxylic and aromatic acids, terpenes, and phenols. The peak at 1579 cm^{-1} has a significant effect due to aromatic components, and those at 630 and 465 cm^{-1}, attributed to the stretching of the Zn-O bond, confirm the formation of G-ZnO NPs. It is the exact imprinting of the biological components of Zingiber officinale present on the surface of the nanoparticles [25,26].

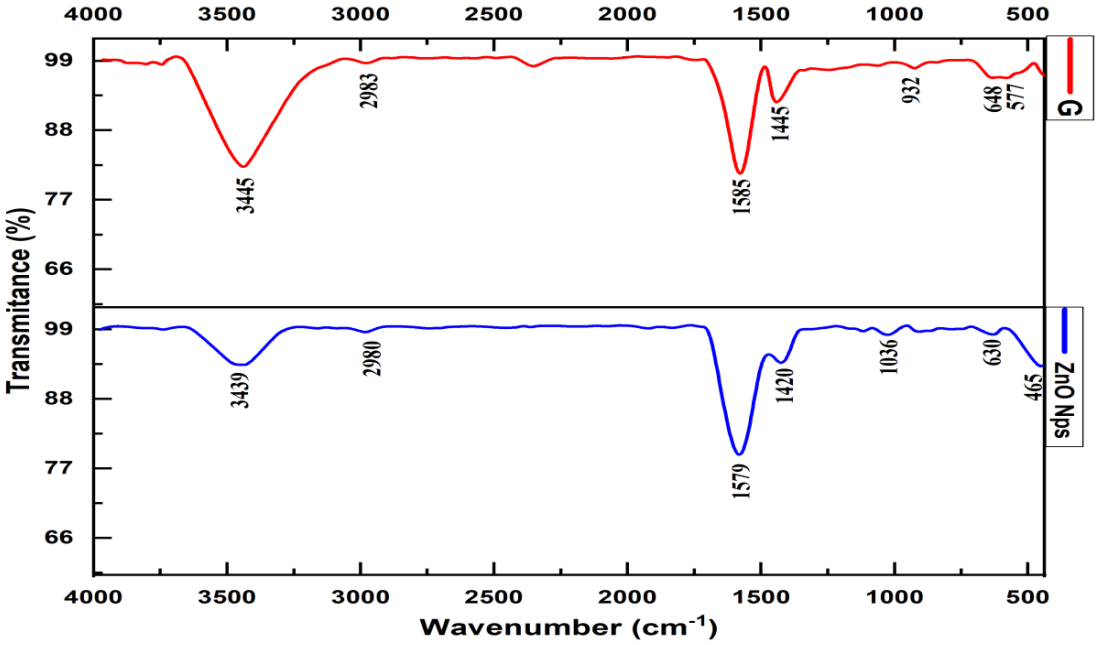

Figure 4: FTIR spectra of Zingiber officinale before and after the formation of ZnO nanoparticles.

The FTIR analysis of Syzygium aromaticum extract was done as shown in Figure 5, and the wave numbers and their functional groups were set as given in Table 2. FTIR screening of pre-synthesized S-ZnO NPs validated the functions of Syzygium aromaticum extract as a reducing agent and covering agent. Figure 5 displays broadband coupling for OH expansion vibrations at 3448 cm^{-1}. The peaks are observed at 2347, 1580, 1382, 1025, 650, and 470 cm^{-1}. One can note the presence of organic compounds, various types of ester, aromatic, methyl, and amino acid. The peak at 1580 cm^{-1} has a significant effect due to the aromatic components, and those at 650 and 470 cm^{-1} are attributed to the stretching of the Zn-O bond

and confirm the formation of S-ZnO NPs. It is the exact imprinting of the biological components of Syzygium aromaticum present on the surface of the nanoparticles[27,28].

Figure 6 illustrates a slight difference in the positions of the peaks of the G-ZnO and that of the S-ZnO samples, which is due to the effect of the plant extract in each sample. It can be seen that the sample G-ZnO has peaks at 1420 cm^{-1} and 2980 cm^{-1}, while the peaks for the S-ZnO sample are located at 1382 cm^{-1} and 2347 cm^{-1}. This difference may be caused by the remaining chemical compounds of the plant and their effect on the matter.

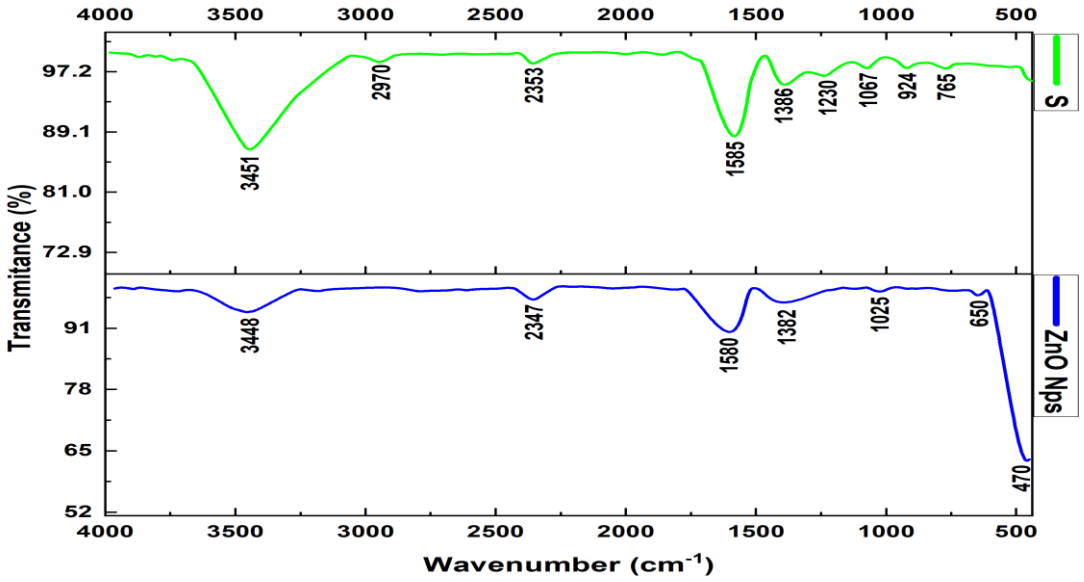

Figure 5: FTIR spectra of Syzygium aromaticum before and after the formation of ZnO nanoparticles.

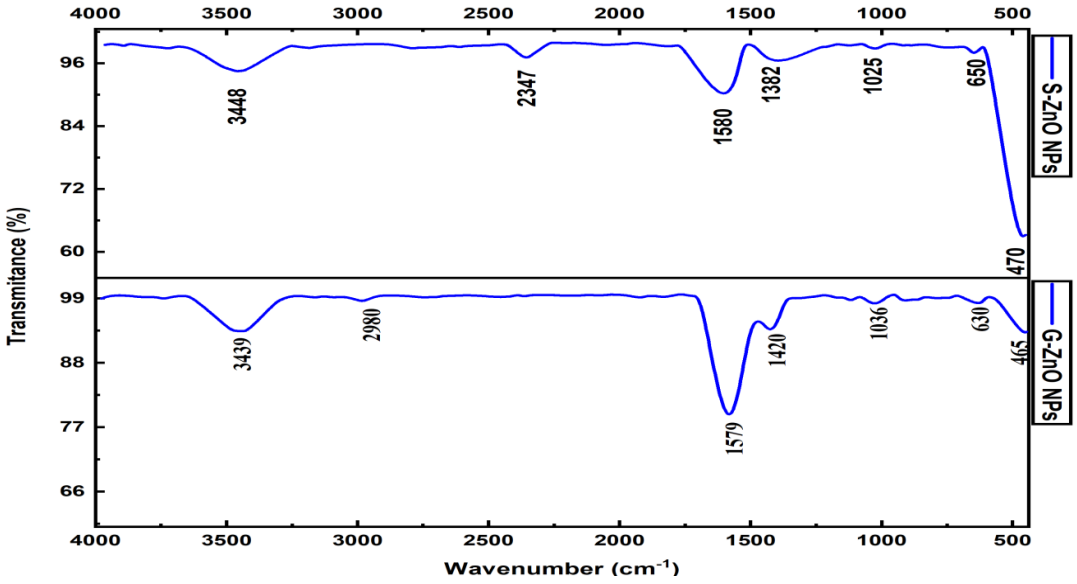

Figure 6: FTIR spectra of G-ZnO nanoparticles and S-ZnO nanoparticles.

Table 2: FTIR spectra of G (Zingiber officinale) and S (Syzygium aromaticum) extract samples groups.

Wavenumber (cm^{-1})	Group	Functional Groups	Reference
3445	OH stretch; H bonded	OH	[29,30]
2983	OH stretch H-bonded	Carboxilyc Acid (RCOOH)	[30,31]
1585	C–H In-plane stretching and deforming	Aromatic skeletal stretching of lignin	[32]
1445	Ring aromatic stretch (4p)	Aromatic C=C	[24,29,30]
932	C=C	Terpenes like zingiberene, β-elemene, limonene present , camphene	[32,33]
648	O=H bond	Phenol	[29,30]
577	C-Br		[2,34]
S (Syzygium aromaticum)			
Wavenumber (cm^{-1})	**Group**	**Functional Groups**	**Reference**
3451	O-H	carboxylic	[27, 35]
2970	CH stretch (sp3)	carboxylic/phenolic	[24, 27]
2353	C-O	ester group	[27]
1585	C=C	Aromatic skeletal stretching of lignin	[32, 36]
1386	(CH3)	methyl groups	[27]
1230	(CH3)	methyl groups	[27]
1067	C-H	amino acid	[36]
924	C-H	Limonene	[28]
765	CH2	eugenol groups	[27]

The optical properties of G-ZnO and S-ZnO NPs as powders produced by green synthesis were evaluated using diffuse reflection spectroscopy. Figures 7a and 8a showed the absorbance spectra at 300-800nm wavelength range for both prepared ZnO NPs samples. In general, one can note that the absorbance value of S-ZnO NPs is higher than that of G-ZnO NPs in all wavelengths. The absorbance of both is low at wavelengths more than 400 nm. The excitonic absorption peaks were between 300 and 400 nm (359 nm for G-ZnO and 361 nm for S-ZnO), typical characteristics of ZnO NPs peaks, thus confirming their presence. Figures 7b and 8b show the sample reflectance spectra in the 350–500 nm spectral region. The reflectance of the S-ZnO NPs sample has a higher value than that of the G-ZnO NPs sample in the spectral region (400-500 nm). The reflectance of both is low at wavelengths less than 375 nm. The recorded reflection can be transformed into absorption using the Kobelka-Munch equation[37]:

$$F(R) = \frac{k}{s} = \frac{(1-R)^2}{2R} \quad 2$$

Where: F(R) is the Kubelka–Munk function corresponding to the absorbance, K/S is the ratio of the absorption coefficient to the scattering coefficient, and R is the diffuse reflectance (%). The band gap energy (E_g) of the material and the type of optical transition between the valence band and conduction band were evaluated using the following modified K–M equation:

$$(F(R)hv) = A(hv + Eg)^n \quad 3$$

Where: *A is a* constant that depends on the transition probability and measures the disorder of the material and band tailing, *hv* is the photon energy, and the exponent factor *n* is related to the nature of the optical transition. The value of *n* equals 1/2 for the allowed direct band gap, 2 for the allowed indirect band gap, 3/2 for the forbidden direct band gap and 3 for the forbidden indirect band gap [38].

The ultraviolet and visible diffuse reflectance spectra of G-ZnO NPs and S-ZnO NPs

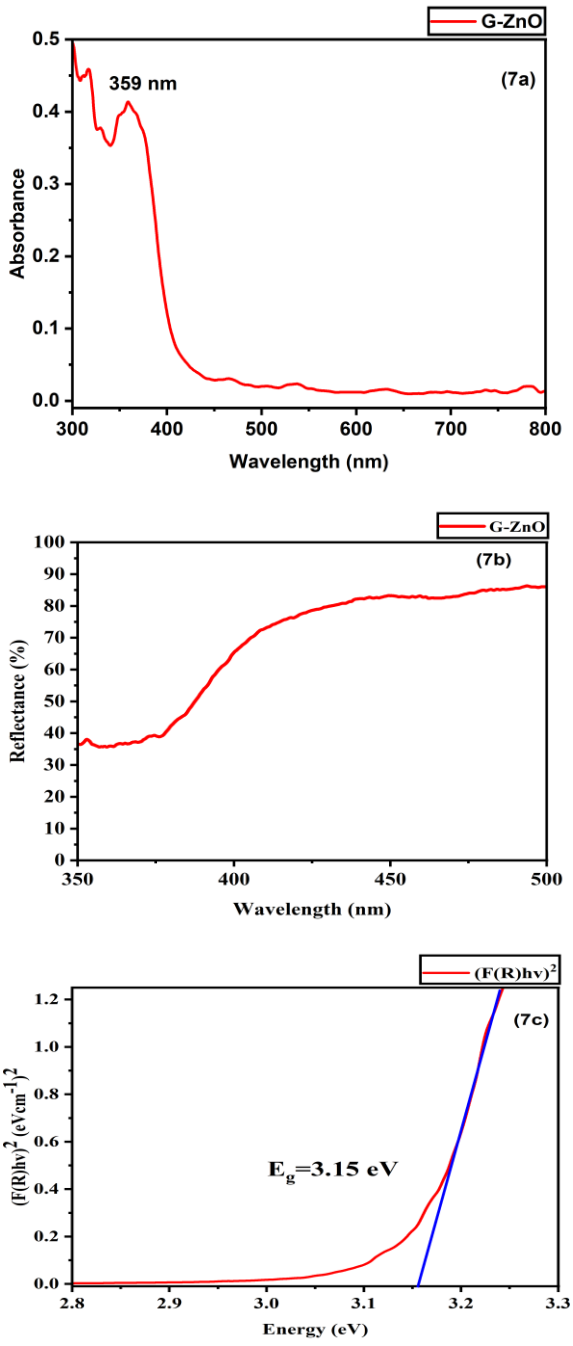

Figure 7: (a) Asorbance vs. wavelength (b) Reflectance vs. wavelength , (c) Variation of $(F(R)hv)^2$ vs energy of G-ZnO.

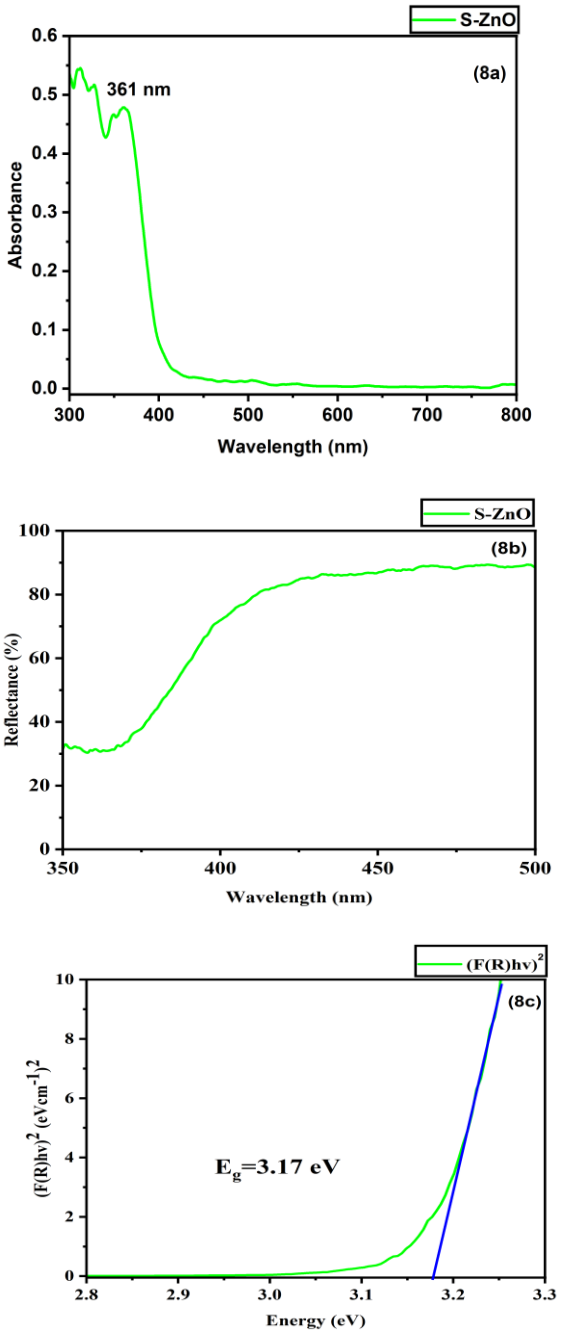

Figure 8: (a) Absorbance vs. wavelength (b) Reflectance vs. wavelength , (c) Variation of $(F(R)hv)^2$ vs energy of S-ZnO.

are shown in Figures 7c and 8c. The energy gap for G-ZnO and S- ZnO samples was allowed a direct energy gap and nearly similar values (3.15 eV and 3.17 eV).

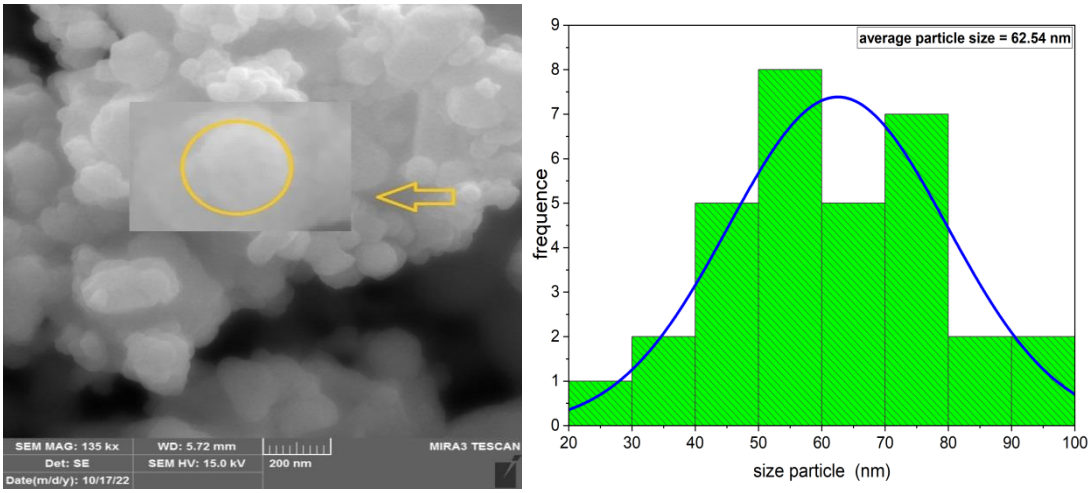

Figure 9: SEM micrograph of the synthesized G-ZnO NPs and composition using EDX.

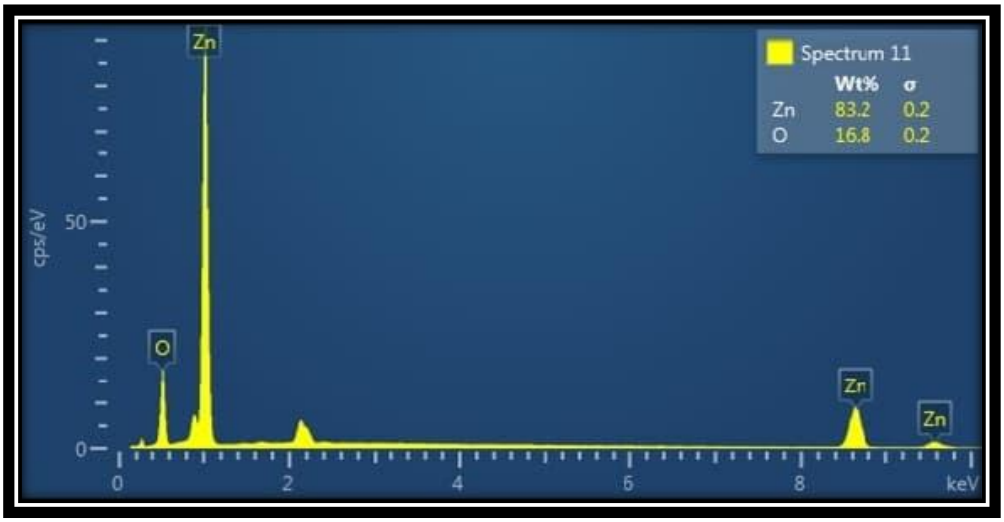

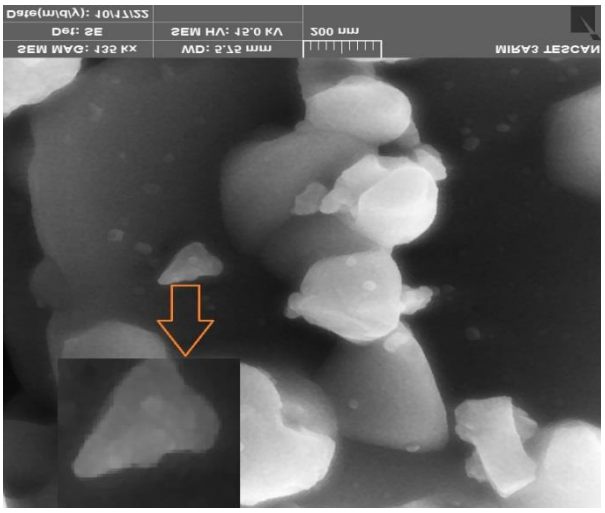

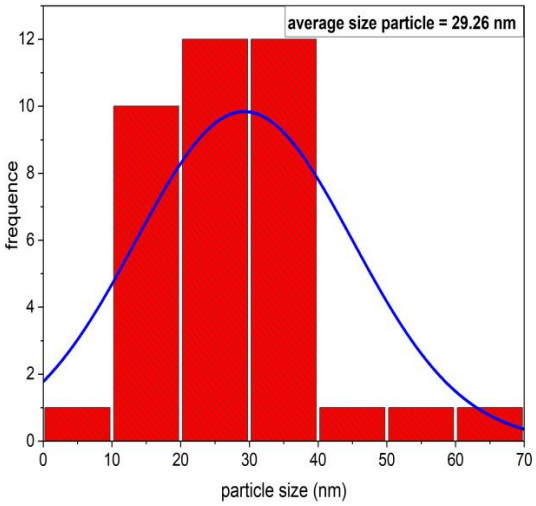

Figure 10: SEM micrograph of the synthesized S-ZnO NPs and composition using EDX

The morphological characteristics of the nanoparticles prepared with Zingier officinale and Syzygium aromaticum were studied by scanning electron microscopy. G-ZnO and S-ZnO nanoparticles appeared to be agglomerated, triangular, spherical and of various other shapes, as shown in Figures 9 and 10, respectively. The average size of G-ZnO and S-ZnO nanoparticles was calculated, which was about 26.92 nm (note that the particles range in size from 10 nm to 40 nm) and 62.45 nm (the particle size ranges from 40 nm to 80 nm), respectively, with microstructures of 200nm length. Purity and composition of the prepared ZnO was checked by EDX. One can observe the three pure peaks for Zn and O, located from 1 to 10 keV, which were also previously reported for the synthesis of ZnO nanoparticles [39].

Antibacterial Activity

ZnO NPs reduces the activity of a wide range of bacteria strains (mainly gram-positive and gram-negative) without antibiotics. Figure 11 and Table 4 show the effect of G-ZnO and S-ZnO on Staphylococcus aureus (S. aureus), Escherichia coli (E. coli) , and Bacillus subtilis (B. subtilis). The statistical representation of the results is shown in Figure 12. It can be seen that the effect of G-ZnO on the bacteria is better than that of S-ZnO, as shown in Figure 12. This effect may be due to the difference in the size and shape of the zinc nanoparticles synthesised by the green method using both plant extracts. G-ZnO had an apparent effect on the bacteria (note that the nanoparticles ranged in size from 10 nm to 40 nm) and that the

average size of nanoparticles was 26.92 nm. The S-ZnO nanoparticles ranged in size from 40 nm to 80 nm, with an average size of 62.45 nm. Their effect was clear on the bacteria but less than the previous one. This may be due to the difference in the sizes of the nanoparticals, which is a major reason for the effect on the bacteria. The nanoparticles size easily penetrate the cell wall and reach the nucleus. This agrees with the results of Martínez-Castañón et al. [40]. Also, the different shapes of the nanoparticles, due to the active role of plant extracts and the chemical compounds, affects the biological efficiency; for example, the G-ZnO nanoparticles are of triangular shape while the S-ZnO nanoparticles are of spherical shape. The triangular-shaped nanoparticles show better interaction with the cell membrane of bacteria and hence increase toxicity compared to spherical-shaped nanoparticles[41]. The reason that nanoparticles target pathogenic bacteria is due to their large surface area relative to volume; the smaller the size of the nanoparticles, the greater the surface area of the zinc nanoparticles, which contributes to an increase in the charge on the surface, which leads to a higher killing or inhibition ratio towards bacteria due to the electrostatic attraction [40,42].

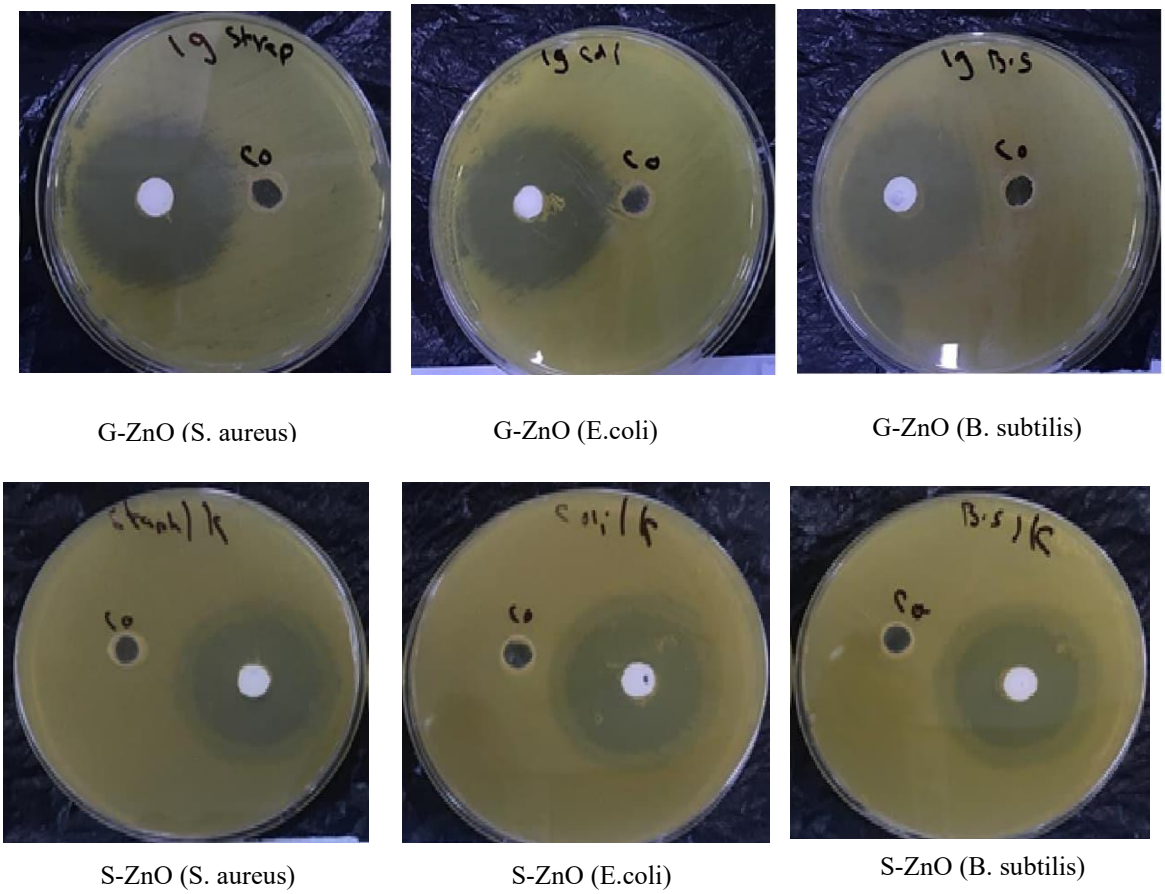

Figure 11: Antibacterial activity of G-ZnO and S-ZnO NPs against Staphylococcus aureus (S. aureus), Escherichia coli (E. coli), and Bacillus subtilis (B. subtilis)

Table 4 : The bacteria used in the study and the effect of zinc nanoparticles on each type of bacteria.

Bacterial	G-ZnO	S-ZnO	Type
S. aureus	30	24	Gram-positive bacterium
E.coli	31	24	Gram-negative bacterium
B. subtilis	28	23	Gram-positive bacterium

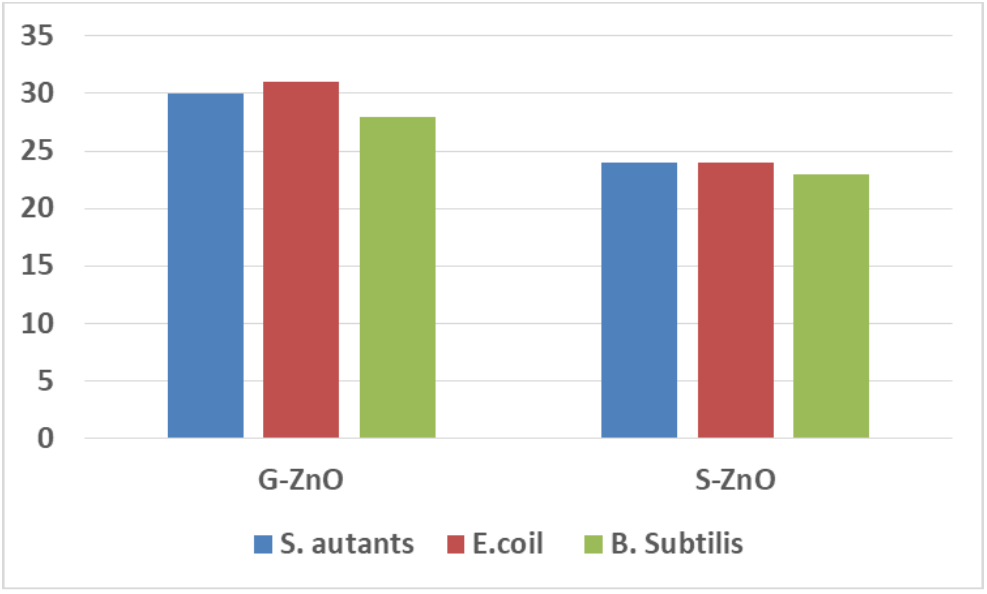

Figure 12: Antibacterial activity of 100 µg/ml G-ZnO NPs and S-ZnO NPs ,for Staphylococcus aureus (S. aureus), Escherichia coli (E. coli), and Bacillus subtilis (B.

4. Conclusions

Zinc oxide nanoparticles were synthesized successfully using an eco-friendly, simple and low-cost method from Zingiber officinale and Syzygium aromaticum extract with Zn $(NO_3)_2$,$6H_2O$ aqueous solution. The physical examinations of prepared G-ZnO and S-ZnO showed that the nanoparticle structures were different in shape and size, due to differences in the chemical composition of both plant extracts. The size and shape played a role in their effective antibacterial activity. ZnO nanoparticles showed significant bactericidal effects against both gram-positive and gram-negative, where G-ZnO showed a more significant effect than S-ZnO.

References

[1] N. Elavarasan, K. Kokila, G. Inbasekar, and V. Sujatha, "Evaluation of photocatalytic activity, antibacterial and cytotoxic effects of green synthesized ZnO nanoparticles by sechium edule leaf extract," *Research on Chemical Intermediates*, vol. 43, no. 5, pp. 3361–3376, 2016. doi:10.1007/s11164-016-2830-2.

[2] I. lashin, M. Hasanin, S. A. Hassan, and A. H. Hashem, "Green biosynthesis of zinc and selenium oxide nanoparticles using callus extract of ziziphus spina-christi: characterization, antimicrobial, and antioxidant activity," *Biomass Conversion and Biorefinery*, vol. 13, no. 11, pp. 10133–10146, 2021. doi:10.1007/s13399-021-01873-4.

[3] M. A. Atiya, A. K. Hassan, and F. Q. Kadhim, "Green synthesis of copper nanoparticles using tea leaves extract to remove ciprofloxacin (CIP) from aqueous media," *Iraqi J. Sci*., vol. 62, no. 9, pp. 2833–2854, 2021, doi: 10.24996/ijs.2021.62.9.1.

[4] S. M. Abed, Y. S. Mahmood, I. F. Waheed, and A. M. Alwan, "Antibacterial activity of green synthesized copper oxide nanoparticles," *Iraqi J. Sci*., vol. 62, no. 9, pp. 3372–3383, 2021, doi: 10.24996/ijs.2021.62.9(SI).8.

[5] I. Hussain, N. B. Singh, A. Singh, H. Singh, and S. C. Singh, "Green synthesis of nanoparticles and its potential application," *Biotechnology Letters*, vol. 38, no. 4, pp. 545–560, 2015. doi:10.1007/s10529-015-2026-7.

[6] H. A. Hessain and J. J. Hassan, "Green synthesis of reduced graphene oxide using ascorbic acid," *Iraqi J. Sci.*, vol. 61, no. 6, pp. 1313–1319, 2020, doi: 10.24996/ijs.2020.61.6.9.

[7] L. Umaralikhan and M. J. Jaffar, "Green synthesis of ZnO and Mg doped ZnO nanoparticles, and its optical properties," *Journal of Materials Science: Materials in Electronics*, vol. 28, no. 11, pp. 7677–7685, 2017. doi:10.1007/s10854-017-6461-1.

[8] M. Batool, S. Khurshid, Z. Qureshi, and W. M. Daoush, "Adsorption, antimicrobial and wound healing activities of biosynthesised zinc oxide nanoparticles," *Chemical Papers,* vol. 75, no. 3, pp. 893–907, 2020. doi:10.1007/s11696-020-01343-7.

[9] S. Sarkar, N. T. Ponce, A. Banerjee, R. Bandopadhyay, S. Rajendran, and E. Lichtfouse, "Green polymeric nanomaterials for the photocatalytic degradation of dyes: A review," *Environmental Chemistry Letters,* vol. 18, no. 5, pp. 1569–1580, 2020. doi:10.1007/s10311-020-01021-w.

[10] S. Fakhari, M. Jamzad, and H. Kabiri Fard, "Green synthesis of zinc oxide nanoparticles: A comparison," *Green Chemistry Letters and Reviews,* vol. 12, no. 1, pp. 19–24, 2019. doi:10.1080/17518253.2018.1547925.

[11] A. M. Sadaa and Z. T. Al Abdullah, "Green synthesis of nickel nanoparticles and their application of removal of aliphatic hydrocarbons from crude oil," *Iraqi J. Sci.*, vol. 62, no. 11, pp. 4333–4341, 2021, doi: 10.24996/ijs.2021.62.11(SI).14.

[12] K. A. Aadim and I. K. Abbas, "Synthesis and investigation of the structural characteristics of zinc oxide nanoparticles produced by an atmospheric plasma jet," *Iraqi J. Sci.*, vol. 64, no. 4, pp. 1743–1752, 2023. doi:10.24996/ijs.2023.64.4.15.

[13] M. F. A. Alias, Kh. M. Rashid, and K. A. Adem, "Optical properties for TI doped thin ZnO films prepared by PLD," *International Journal of Innovative Research in Science, Engineering and Technology,* vol. 03, no. 08, pp. 15538–15544, 2014. doi:10.15680/ijirset.2014.0308064.

[14] J. Jiang, J. Pi, and J. Cai, "The advancing of zinc oxide nanoparticles for biomedical applications," *Bioinorganic Chemistry and Applications,* vol. 2018, pp. 1–18, 2018. doi:10.1155/2018/1062562.

[15] G. Madhumitha, G. Elango, and S. M. Roopan, "Biotechnological aspects of ZnO nanoparticles: overview on synthesis and its applications," *Applied Microbiology and Biotechnology,* vol. 100, no. 2, pp. 571–581, 2015. doi:10.1007/s00253-015-7108-x.

[16] T. J. Webster and I. Seil, "Antimicrobial applications of nanotechnology: methods and literature," *International Journal of Nanomedicine*, vol.7 , pp. 2767–2781, 2012. doi:10.2147/ijn.s24805.

[17] M. Ali, M. Ikram, M. Ijaz, A. Ui-Hamid, M. Avais, and A. A. Anjum "Green synthesis and evaluation of n-type ZnO nanoparticles doped with plant extract for use as alternative antibacterials," *Applied Nanoscience,* vol. 10, no. 10, pp. 3787–3803, 2020. doi:10.1007/s13204-020-01451-6.

[18] A. Umamaheswari, S. L. Prabu, S. A. John, and A. Puratchikody, "Green synthesis of zinc oxide nanoparticles using leaf extracts of raphanus sativus var. longipinnatus and evaluation of their anticancer property in A549 cell lines," *Biotechnology Reports,* vol. 29, pp. 1-9, 2021. doi:10.1016/j.btre.2021.e00595.

[19] M. Aminuzzaman, L. P. Ying, W.-S. Goh, and A. Watanabe, "Green synthesis of zinc oxide nanoparticles using aqueous extract of garcinia mangostana fruit pericarp and their photocatalytic activity," *Bulletin of Materials Science*, vol. 41, no. 2, pp. 1-10, 2018. doi:10.1007/s12034-018-1568-4.

[20] A. C. Janaki, E. Sailatha, and S. Gunasekaran, "Synthesis, characteristics and antimicrobial activity of ZnO nanoparticles," *Spectrochimica Acta Part A: Molecular and Biomolecular Spectroscop*y, vol. 144, pp. 17–22, 2015. doi:10.1016/j.saa.2015.02.041.

[21] R. A. Rasheed and M. F. Alias, "The role of aluminum doping on structural and optical properties of ZnO thin films prepared by PLD," *IOP Conference Series: Materials Science and Engineering,* vol. 757, no. 1, pp. 1-11, 2020. doi:10.1088/1757-899x/757/1/012056.

[22] M. Ramesh, M. Anbuvannan, and G. Viruthagiri, "Green synthesis of ZnO nanoparticles using solanum nigrum leaf extract and their antibacterial activity," *Spectrochimica Acta Part A: Molecular and Biomolecular Spectroscopy,* vol. 136, pp. 864–870, 2015. doi:10.1016/j.saa.2014.09.105.

[23] B. H. Shnawa, S. M. Hamad, A. A. Barzinjy, P. A. Kareem, and M. H. Ahmed, "Scolicidal activity of biosynthesized zinc oxide nanoparticles by Mentha longifolia L. leaves against Echinococcus granulosus protoscolices," *Emergent Materials,* vol. 5, no. 3, pp. 683–693, 2021. doi:10.1007/s42247-021-00264-9.

[24] A. B. Nandiyanto, R. Oktiani, and R. Ragadhita, "How to read and interpret FTIR spectroscope of organic material," *Indonesian Journal of Science and Technology,* vol. 4, no. 1, pp. 97-118, 2019. doi:10.17509/ijost.v4i1.15806.

[25] P. G. Daswani, S. Brijesh, P. Tetali, N. H. Antia, and T. J. Birdi, "Antidiarrhoeal activity of zingiber officinale (Rosc.)," *Curr. Sci.,* vol. 98, no. 2, pp. 222–229, 2010.

[26] K. S. Khashan, G. M. Sulaiman, and S. A. Hussain, "Synthesis and characterization of aluminum doped zinc oxide nanostructures by Nd:YAG laser in liquid," *Iraqi J. Sci*., vol. 61, no. 10, pp. 2590–2598, 2020, doi: 10.24996/ijs.2020.61.10.15.

[27] P. Parthipan, M. S. AlSalhi, S. Devanesan, and A. Rajasekar, "Evaluation of syzygium aromaticum aqueous extract as an eco-friendly inhibitor for microbiologically influenced corrosion of carbon steel in oil reservoir environment," *Bioprocess and Biosystems Engineering,* vol. 44, no. 7, pp. 1441–1452, 2021. doi:10.1007/s00449-021-02524-8.

[28] M. Anvarinezhad, A. Javadi, and H. Jafarizadeh-Malmiri, "Green approach in fabrication of photocatalytic, antimicrobial, and antioxidant zinc oxide nanoparticles – hydrothermal synthesis using clove hydroalcoholic extract and optimization of the process," *Green Processing and Synthesis,* vol. 9, no. 1, pp. 375–385, 2020. doi:10.1515/gps-2020-0040.

[29] H. Purnomo, F. Jaya, and S. B. Widjanarko, "The effects of type and time of thermal processing on ginger (zingiber officinale roscoe) rhizome antioxidant compounds and its quality," *Int. Food Res. J.*, vol. 17, no. 2, pp. 335–347, 2010.

[30] A. H. Alkhathlan, H. A. Al-Abduikarimkh, K. Merajuddin, K. Mujeeb, M. Alkholief, A. Alshamsan, A. Almomen, N. Alberkairi, H. Z. Alkhathlan, and M. R. H.Siddiqui, "Evaluation of the anticancer activity of phytomolecules conjugated gold nanoparticles synthesized by aqueous extracts of zingiber officinale (ginger) and nigella sativa L. seeds (black cumin)," *Materials,* vol. 14, no. 12, pp. 1-17, 2021. doi:10.3390/ma14123368.

[31] A. Devi, V. K. Das, and D. Deka, "Ginger extract as a nature based robust additive and its influence on the oxidation stability of biodiesel synthesized from non-edible oil," *Fuel,* vol. 187, pp. 306–314, 2017. doi:10.1016/j.fuel.2016.09.063.

[32] I. K. Amponsah, A. Boakye, E. Orman, F. A. Armah, L. S. Borquaye, S. Adjei, Y. A. Dwamena, K. A. Baah, and B. K. Harley , "Assessment of some quality parameters and chemometric-assisted FTIR spectral analysis of commercial powdered ginger products on the Ghanaian market," *Heliyon*, vol. 8, no. 3, pp. 1-9, 2022. doi:10.1016/j.heliyon.2022.e09150.

[33] U. K. Hussein, N. E. Y. Hassan, M. E. A. Elhalwagy, A. R. Zaki, H.O. Abubakr, k. C. N. Venkata, K.Y. Jang, and A. Bishayee , "Ginger and propolis exert neuroprotective effects against monosodium glutamate-induced neurotoxicity in rats," *Molecules*, vol. 22, no. 11, pp. 1928, 2017. doi:10.3390/molecules22111928.

[34] Archana, A. Kr. Aman, R. Kr. Singh, N. Kr., and A. Jabeen, "Effect of superfine grinding on structural, morphological and antioxidant properties of ginger (zingiber officinale) nano crystalline food powder," *Materials Today: Proceedings,* vol. 43, pp. 3397–3403, 2021. doi:10.1016/j.matpr.2020.09.028.

[35] A. N. Chaudhari and A. G. Ingale, "Syzygium aromaticum extract mediated, rapid and facile biogenic synthesis of shape-controlled (3D) silver nanocubes," *Bioprocess and Biosystems Engineering,* vol. 39, no. 6, pp. 883–891, 2016. doi:10.1007/s00449-016-1567-z .

[36] S. Yedurkar, C. Maurya, and P. Mahanwar, "Biosynthesis of zinc oxide nanoparticles using ixora coccinea leaf extract-a green approach," *Open Journal of Synthesis Theory and Applications*, vol. 05, no. 01, pp. 1–14, 2016. doi:10.4236/ojsta.2016.51001.

[37] S. S. Abdullahi, S. Güner, Y. Koseoglu, I. M. Musa, B. I. Adamu, and M. Abdulhamid, "Sımple method for the determınatıon of band gap of a nanopowdered sample usıng kubelka munk theory," *J. Niger. Assoc. Math. Phys.*, vol. 35, pp. 241–246, 2016.

[38] T. S. Aldeen, H. E. Ahmed Mohamed, and M. Maaza, " ZnO nanoparticles prepared via a green synthesis approach: physical properties,photocatalytic and antibacterial activity," *Journal of Physics and Chemistry of Solids,* vol. 160, pp. 1-12, 2022. doi:10.1016/j.jpcs.2021.110313.

[39] I.-M. Chung, A. A. Rahuman, S. Marimuthu, A. V. Kirthi, K. Anbarasan, and G. Rajakumar, "An investigation of the cytotoxicity and caspase-mediated apoptotic effect of green synthesized zinc oxide nanoparticles using eclipta prostrata on human liver carcinoma cells," *Nanomaterials,* vol. 5, no. 3, pp. 1317–1330, 2015. doi:10.3390/nano5031317.

[40] G. A. Martínez-Castañón, N. Niño-Martínez, F. Martínez-Gutierrez, J. R. Martínez-Mendoza, and F. Ruiz, "Synthesis and antibacterial activity of silver nanoparticles with different sizes," *Journal of Nanoparticle Research*, vol. 10, no. 8, pp. 1343–1348, 2008. doi:10.1007/s11051-008-9428-6.

[41] H. Agarwal, S. Menon, S. Venkat Kumar, and S. Rajeshkumar, "Mechanistic study on antibacterial action of zinc oxide nanoparticles synthesized using green route," *Chemico-Biological Interactions,* vol. 286, pp. 60–70, 2018. doi:10.1016/j.cbi.2018.03.008.

[42] M. F. Alias and A. S. Abd - Alsada, "The influence of zinc oxide with carbon nanotube composite nanomaterials on antibacterial activity," *Journal of Physics: Conference Series*, vol. 2114, no. 1, pp. 012089, 2021. doi:10.1088/1742-6596/2114/1/012089.